Acta Cryst. (1996). A52, 621–628

Position-Resolved Measurement of the Polarization State in the Forward-Diffracted X-ray Beam

WOLFRAM LEITENBERGER, CHRISTIAN EISENSCHMIDT AND HANS-REINER HÖCHE

Fachbereich Physik, Martin-Luther-Universität Halle-Wittenberg, Friedemann-Bach-Platz 6, D-06108 Halle(Saale), Germany

(Received 7 July 1995; accepted 7 February 1996)

Abstract

The polarization state in narrow regions of the transmitted (forward-diffracted) beam in Laue-case dynamical X-ray diffraction inside the so-called Borrmann fan was determined experimentally. The polarization state at each point of the Borrmann fan depends on the phase difference between the mutually perpendicularly polarized waves. It additionally depends on the ratio of its amplitudes, which are influenced by the *Pendellösung* oscillations resulting from the Borrmann effect. The change from a linearly polarized incident wave into an elliptically polarized wave was measured as a function of its position in the Borrmann fan by a polarization analyser. The 'polarization-resolved' *Pendellösung* intensities in the transmitted beam were observed. The measurements were made on the symmetrical $\bar{2}20$ Laue reflection of a parallel-sided perfect Si (111) crystal using monochromatic linearly polarized synchrotron radiation. Calculations according to the dynamical theory were compared with the measurements.

1. Introduction

The polarization of X-rays has been known since early investigations of X-ray scattering. Later, it was shown that polarization phenomena occur that are similar to those observed with visible light. The polarization phenomena on the basis of dynamical X-ray diffraction are used for generation and analysis of polarized X-rays in X-ray spectroscopy or X-ray magnetic scattering. For some years, synchrotron radiation has allowed measurement of difficult to detect dynamical effects. Polarization phenomena according to the dynamical theory have been investigated by a number of authors. The polarization phenomena in Laue-case X-ray diffraction can be measured by direct and indirect methods. By indirect methods, the intensities are detected without separating the two polarization states, *e.g.* observation of *Pendellösung* fringes. By direct methods, the polarization state is determined using a polarizer–analyser arrangement.

The first *Pendellösung* experiments by Kato & Lang (1959) with a wedge-shaped crystal were explained by the spherical-wave theory developed by Kato (1961). Hattori, Kuriyama & Kato (1965) and Hart & Lang (1965) made the same experiments using linearly polarized radiation. The fading effect occurring for unpolarized radiation could be explained as a superposition of two sets of fringes with different spacing originating from two mutually perpendicularly polarized wavefields. Skalicky & Malgrange (1972) also observed the fading in the case of a linearly polarized incident wave, where the polarization vector inclines at an angle of 45° with respect to the diffraction plane. The integrated intensity over the whole Borrmann fan in the diffracted H beam was detected as a function of crystal thickness. For thick crystals, the main contribution to the intensity comes from the centre of the Borrmann fan as a result of anomalous absorption. The phase relation between the two coherently excited mutually perpendicularly polarized wavefields was used to explain the experimental results. In this way, it was shown that arbitrarily polarized waves can be generated from linearly polarized ones using Laue reflection. All these experiments are based on indirect methods and were performed with an incident spherical wave. Brümmer, Eisenschmidt & Höche (1982) generated elliptically polarized X-rays from linearly polarized ones using an Si quarter-wave plate in Laue geometry. An analyser arrangement was used for the direct measurement of the polarization state.

The polarization state of the 0 beam in the Laue case was measured by Cole, Chambers & Wood (1961). They used the dichroism, the stronger absorption of the π-polarized wavefield, for generating linearly σ-polarized radiation from an X-ray tube. For the direct measurement of the polarization state, they used a Bragg reflection with $2\Theta_B = 90.0°$ as analyser. A more sophisticated experimental arrangement for a tuneable transmission-type X-ray phase retarder in Laue transmission geometry was realized and discussed by Hirano, Ishikawa, Nakamura, Mizutani & Kikuta (1994) using synchrotron radiation. The Borrmann effect in a thick crystal gives priority to the radiation

coming from the centre of the Borrmann fan. The phase shift between the mutually perpendicularly polarized components originating from each branch of the dispersion surface depends on the effective thickness of the crystal.

In view of the application of a phase retarder, the transmitted 0 beam is more favourable. An experimental arrangement like an optical bench is applicable for synchrotron-radiation experiments, where the wavelength is easily tuneable. Since the work of Belyakov & Dmitrienko (1989), the phase shift in Bragg and Laue transmission geometry has been investigated. The authors discussed the polarization state of a transmitted X-ray beam in relation to the deviation from the Bragg angle. Hirano, Izumi, Ishikawa, Anaka & Kikuta (1991) used a thin Si crystal plate to realize a Bragg transmission phase retarder in order to convert linearly polarized radiation into circularly polarized radiation.

The above-mentioned Bragg experiments are restricted to measuring the transmitted waves originating from a small region of the dispersion surface. Selection of this region is made by well collimated incident radiation or by anomalous strong absorption of the branch 2 wavefield. In both cases, the experiments can be interpreted as plane-wave experiments.

Our experiment is dedicated to the direct measurement of the polarization state inside the Borrmann fan of the 0 beam of a relatively thin and weakly absorbing crystal. In this case, all parts of the dispersion surface contribute to the transmitted intensities and the margin regions cannot be neglected. The phase shifting and the intensity ratio of both perpendicularly polarized wavefields are changed in a complicated manner. The maximum phase shift is in the centre of the fan and it decreases at the border. In order to achieve a high local resolution, a narrow incident beam is necessary to prevent blurring of both the polarization state and the intensity oscillations by overlapping of several Borrmann fans that would be exited at different points of the crystal entrance surface. For high local resolution, an additional narrow slit is necessary behind the sample. This is for separating the region of the fan, for which a polarization analysis should be made. By this selection, the experiment can be interpreted like a plane-wave experiment.

2. Theoretical background

The dynamical theory of X-ray diffraction describes the propagation of wavefields in perfect crystals. In the two-beam case, the forward-diffracted 0 wave and the reflected H wave spread out in the crystal. In general, each of these wavefields consists of four linearly polarized Ewald waves with slightly different $\mathbf{k}$ vectors and two different planes of polarization [parallel, π, or normal, σ, to the diffraction plane; Fig. 1(*a*)]. The waves relating to branches 1 and 2 are absorbed weakly and strongly, respectively. Waves of the same polarization state interfere and cause the well known *Pendellösung* phenomena in the crystal.

The phase difference Φ between the σ- and π-polarized waves after passing a crystal plate is given by the difference of the $\mathbf{k}$ vectors and the path length in the sample. The $\mathbf{k}$-vector difference in the centre of the Borrmann fan is obviously described by the distances of the vertices of the two branches of the dispersion surface for each polarization. These differences are the reciprocal *Pendellösung* distances $\Lambda^{-1}_{\pi(\sigma)}$. The phase difference Φ in the centre of the Borrmann fan after passing a crystal of thickness t is $\Phi_{0,j} = 2\pi(\Lambda^{-1}_{\sigma,j} - \Lambda^{-1}_{\pi,j})t$.

In terms of the plane-wave approximation, Hirano, Ishikawa & Kikuta (1993) give the phase difference in relation to the deviation from the exact reflection

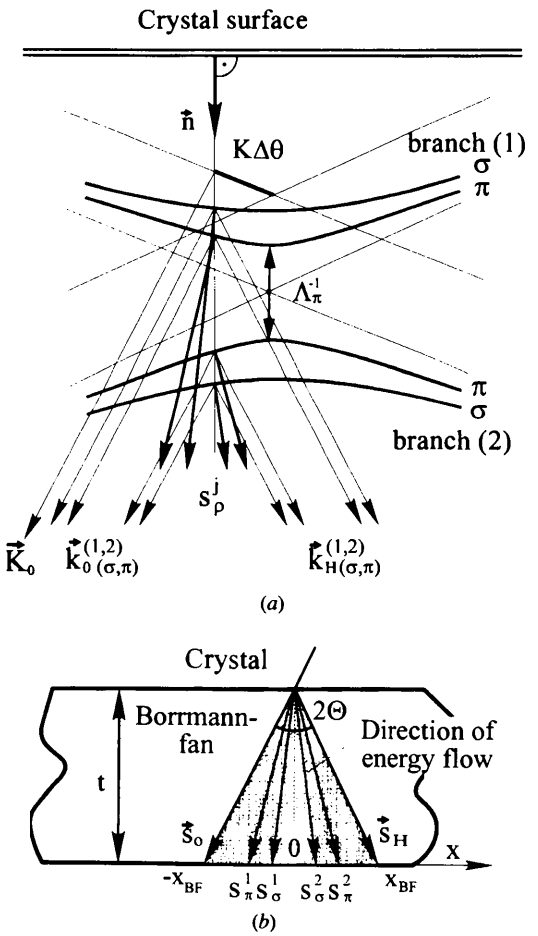

Fig. 1. (*a*) Dispersion surface for the symmetrical Laue case. (*b*) Representation of the direction of energy flow inside the crystal resulting from the tie points plotted in (*a*).

condition corresponding to one branch of the dispersion surface (j) at the crystal exit surface:

$$\Phi_j(\eta) = 2\pi t(\mathbf{k}_{\sigma,j} - \mathbf{k}_{\pi,j}) = [\pi t(\chi_H\chi_{\bar{H}})^{1/2}/\lambda(\gamma_0\gamma_H)^{1/2}] \times [(\eta_{\sigma,j}^2 + 1)^{1/2} - (\eta_{\sigma,j}^2 + \cos^2 2\Theta_B)^{1/2}] \quad (1)$$

with

$$\eta_{\sigma,j}(\Delta\Theta) = [\Delta\Theta \sin(2\Theta_B) + (\chi_{0i}/2)(1 - \gamma_H/\gamma_0)] \times [C(\chi_H\chi_{\bar{H}})^{1/2}(\gamma_H/\gamma_0)^{1/2}]^{-1}.$$

For each incident direction, there exists a small difference in the length of the **k** vectors for the mutually perpendicularly polarized waves (Fig. 1*a*). Here, η is the normalized angle of incidence and the index j signifies branch 1 or 2 of the dispersion surface. Θ_B is the Bragg angle, $\Delta\Theta = \Theta - \Theta_B$ is the deviation from the exact reflection condition, and λ is the wavelength of the incident beam. $\chi_{0(H)}$ are the Fourier coefficients of the complex dielectric susceptibility, χ_{0i} is the imaginary part of χ_0, and γ_0 and γ_H are the cosines of the angles between the directions $\mathbf{k}_0$ and $\mathbf{k}_H$ and the inward-directed normal **n** on the entrance surface. The polarization factor C is unity for the σ component and $\cos 2\Theta_B$ for the π component. The conversion from the deviation parameter η to the corresponding position x in the Borrmann fan on the exit surface is given by the relation

$$x = x_{BF}\eta/(1 + \eta^2)^{1/2} \quad (-\infty < \eta < \infty). \quad (2)$$

As is known from the model of the dispersion surface, there is a definite direction of energy flow inside the crystal for every direction of the incident wave. The direction of energy flow is parallel to the direction of the normal to the dispersion surface, as shown in Fig. 1(*b*). In the symmetrical Laue case, the width of the Borrmann fan on the exit surface is given by $2x_{BF} = 2t \tan\Theta_B$.

The calculations of the intensity distribution at the back of the crystal were carried out on the basis of Takagi's equations (Takagi, 1969). This equation system was solved analytically for the case of a parallel-sided perfect crystal using Riemann's integration method assuming a point wave incident on the crystal surface.

The intensity distributions $I_0(x)$ and $I_H(x)$ on the exit surface of the crystal are given for a symmetric Laue reflection as a function of the distance x from the centre of the Borrmann fan ($-x_{BF} < x < x_{BF}$) by

$$I_0(x) = \left| \frac{K^2\pi^2C^2\chi_H\chi_{\bar{H}}\gamma_0\gamma_H}{\sin^2 2\Theta_B} \frac{x_{BF} - x}{x_{BF} + x} \times J_1^2[(\pi t/2\Lambda)(1 - x^2/x_{BF}^2)^{1/2}]A^2(x) \right|$$
$$I_H(x) = \left| \frac{K^2\pi^2C^2\chi_H\chi_{\bar{H}}\gamma_0\gamma_H}{\sin^2 2\Theta_B} \times J_0^2[(\pi t/2\Lambda)(1 - x^2/x_{BF}^2)^{1/2}]A^2(x) \right|, \quad (3)$$

where

$$\Lambda = (\gamma_0\gamma_H)^{1/2}/[KC(\chi_H\chi_{\bar{H}})^{1/2}]$$

and

$$A(x) = \exp\{-(\mu t/4)[(1/\gamma_0 + 1/\gamma_H) + (x/x_{BF})(1/\gamma_0 - 1/\gamma_H)]\}.$$

The wave vector K is defined by $K = 1/\lambda$. Λ signifies Ewald's *Pendellösung* distance in the centre of the Borrmann fan. It describes both the oscillations (real part of Λ) and the anomalous absorption (imaginary part). The quantity μ is the linear absorption coefficient of the crystal. $J_{i(i=0,1)}$ are Bessel functions of the ith order and the factor $A(x)$ takes into account the absorption.

Fig. 2 shows the calculated phase difference Φ between the two polarized components at the exit surface of an Si (111) crystal of 262 μm thickness for a symmetric $\bar{2}20$ Laue reflection ($\lambda = 1.0$ Å). Furthermore, the intensities of the π and the σ components are drawn as a function of the position $x + x_{BF}$. The oscillations of intensity are a result of the interference between wavefields 1 and 2. The theoretical profiles were convoluted by a slit function of width 15 μm for comparison with experimental results.

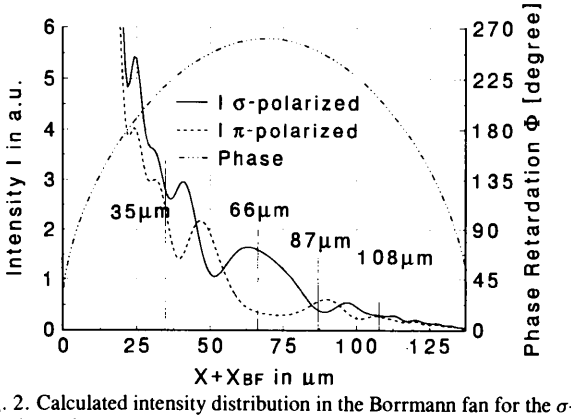

Fig. 2. Calculated intensity distribution in the Borrmann fan for the σ- and π-polarized wavefields and the calculated phase difference on the exit surface of a 262 μm thick Si crystal for the symmetrical $\bar{2}20$ reflection (= 1.0 Å). The vertical solid lines signify the positions where the polarization states were measured.

Calculations of the phase differences were carried out only for the anomalously weakly absorbed waves originating from branch 1 of the dispersion surface. The intensity distribution of the weakly and strongly absorbed waves were additionally calculated separately using equations given by Authier (1970), neglecting the interaction between the two waves. As shown in Fig. 3,

the intensities from branch 2 wavefield are only *ca* 10% of that from branch 1 in the centre of the Borrmann fan. The sign of the phase shift is opposite to that of the weakly absorbed waves. The influence of the strongly absorbed waves on the total polarization state will be discussed later. A defined phase difference between the mutually perpendicularly polarized waves is given for each point at the exit surface in the case of an incident point wave. The polarization state is determined by the phase shift and by the ratio of amplitudes of the waves.

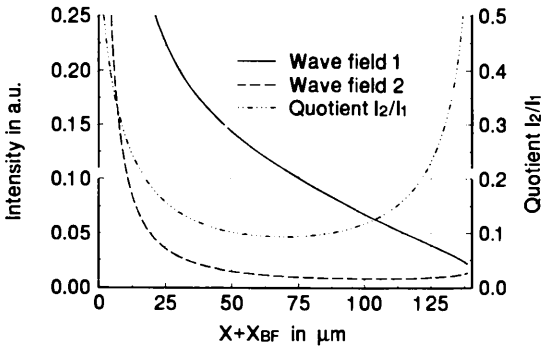

Fig. 3. Separate representation of the intensity distribution in the Borrmann fan for the anomalously weak (1) and the anomalously strong (2) absorbed wavefields for the same conditions as in Fig. 2. The ratio of the intensities I_2/I_1 shows that the Borrmann effect (the anomalous absorption) predominates in the centre of the Borrmann fan.

3. Experimental

The experimental arrangement is shown in Fig. 4(*a*,*b*). The beam delivered by the wiggler BW1 at the DORIS III storage ring at HASYLAB was monochromatized to 1.0 Å by a symmetrical Si (111) double monochromator. In order to suppress higher harmonics, the second monochromator crystal was detuned down to 70% of the maximum intensity. The monochromatized radiation was almost linearly polarized in the orbit plane with a ratio $P = (I_\perp - I_\parallel)/(I_\perp + I_\parallel)$ of 0.93. The intensities $I_\perp$ and $I_\parallel$ were measured by means of scintillation counters measuring the air scattering normal and parallel to the orbit plane after the monochromator. The deviation of the degree of polarization from exact linear polarization is caused by the given beamline characteristics.

An incident 'point wave' at the entrance surface of the sample was realized by the narrow tantalum slit 1 of width 15 μm in front of the crystal. Owing to the 45° inclination of the entrance slit against the orbit plane (see Fig. 4*a*), the entrance slit also passes a small amount of circularly polarized radiation from the off-orbit radiation. The incident beam satisfies the symmetric $\bar{2}20$ Laue reflection in the perfect-crystal Si sample *S*, with $t = 262$ μm, mounted on a goniometer. The divergence of the incident wave was *ca* 30″. Almost the whole dispersion surface was excited when the sample was adjusted into the Laue position. The adjustment of the crystal was controlled by measuring

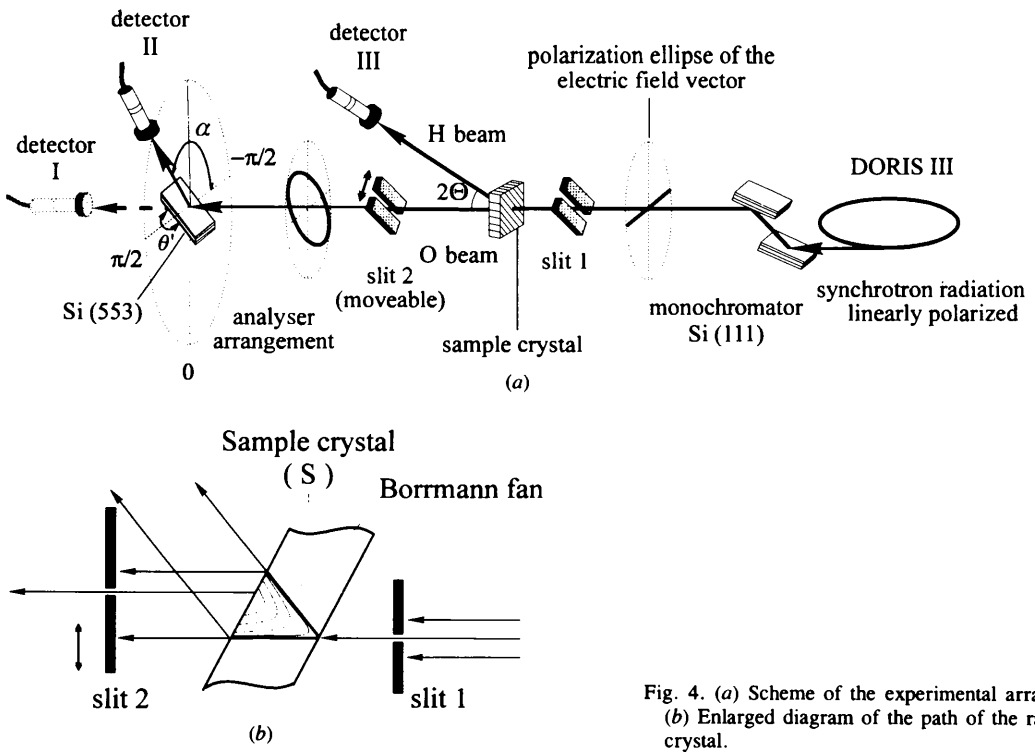

Fig. 4. (*a*) Scheme of the experimental arrangement. (*b*) Enlarged diagram of the path of the rays in the crystal.

the reflected intensity (detector III). The diffraction plane inclines at an angle of 45° with respect to the orbit plane of the storage ring. Thereby, the σ and π components of the waves are excited coherently and with equal amplitudes. A second slit with the same dimensions as slit 1 was placed parallel to the first one 20 mm behind the sample. This slit was moveable with high accuracy in the diffraction plane, as shown in Fig. 4(*b*). The FWHM of the profile of the primary beam was determined to approximately 15 μm by moving slit 2 across the transmitted beam at a fixed position of slit 1. For this, the sample crystal was adjusted far from the Laue position.

When the sample crystal was in the Laue position the intensity profile of the forward-diffracted 0 beam could be detected. The polarization state of the transmitted beam was measured by a simple X-ray polarimeter behind the second slit instead of the scintillation detector I. A perfect-crystal Si 553 analyser was mounted on a two-axis goniometer. The first axis (angle α) was for azimuthal rotation around the beam. The second axis (Θ') was for varying the angle of incidence on the analyser crystal. It allows the measurement of the rocking curve of the symmetrical 553 reflection (Bragg angle 45.0°) by detector II at each azimuthal position α.

3.1. *Determination of the intensity distribution*

With the analyser crystal set into the exact Bragg position Θ'_B, it was possible to make a 'polarization-resolved' measurement of the intensities inside the Borrmann fan for any value of α by scanning slit 2. A direct determination of the polarization state over the whole Borrmann fan is not possible from these measurements because the divergence of the radiation is not constant for the different α values. The measured maximum value is only a coarse measure for the integrated intensity, thereby the measured intensity distributions for different α positions cannot be directly compared against one another. The advantage of this 'polarization-sensitive' measurement, however, is to obtain a qualitative overview about the intensity distribution at the exit surface for a fixed polarization state, *e.g.* the σ- or the π-polarized wavefield separately.

3.2. *Determination of the polarization state*

An exact polarization analysis was made at different positions of slit 2 using integrated intensities of the analyser. The integrated intensities of the 553 Bragg reflection were determined over an α range of more than 270° in steps of 15°. The azimuthal angle α is defined as zero when the diffraction plane of the 553 analyser is normal to the orbit plane. In this way, the diffraction plane is represented by $\alpha = 45°$. All integrated intensities were corrected for background and for the decreasing primary-beam intensities during a synchrotron radiation run by a simultaneously recorded monitor signal.

4. Results and discussion

4.1. *Detection of the intensities in the Borrmann fan*

The intensity profiles across the Borrmann fan were recorded by moving slit 2 and measuring the transmitted intensity with detector I without an analyser crystal. The position of slit 2 was divided by $\cos\Theta$ to compare it with the calculated intensity distribution at the exit surface (the direction of the slit movement is tilted by Θ against the crystal surface). Two examples of intensity profiles are shown in Fig. 5(*a*). A significant increase of the intensity at positions out of the direction of the primary beam was observed by adjusting the crystal *S* into the exact Laue position compared with the measurement for the sample far from this position (1°). In other words, the Borrmann fan was excited. The maximum of the primary beam decreases significantly for *S* at the Laue position because of the exciting of the 0

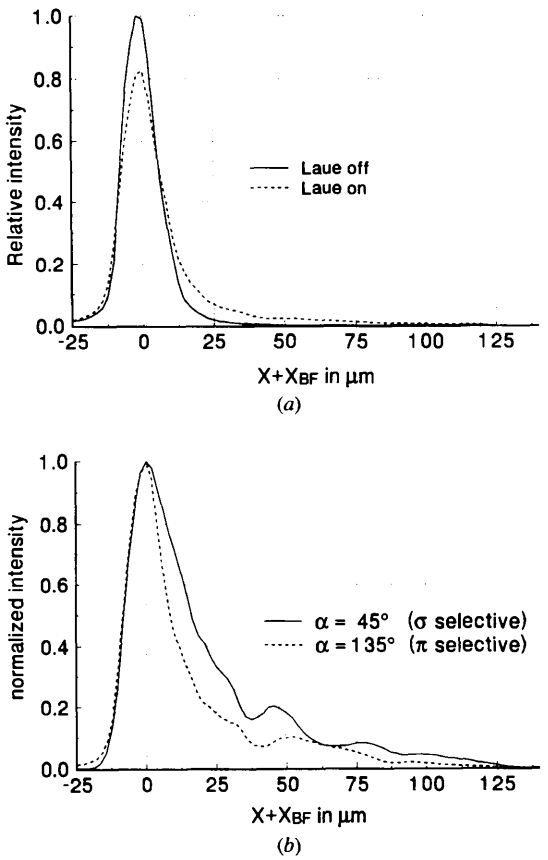

Fig. 5. (*a*) Intensity profile measured by scanning slit 2 with the sample in the off-Laue position (——) and the sample in the Laue position (-----). (*b*) 'Polarization-resolved' Borrmann profile measured with the analyser set to $\alpha = 45$ and $\alpha = 135°$.

and H wavefields. The oscillations of the intensities as a function of the position in the Borrmann fan as calculated from (3) are blurred by at least two factors: (i) the finite width of the slits, and (ii) the simultaneous excitation and detection of the σ and π components. This blurring cannot be reduced in this arrangement.

Two 'polarization-resolved' measurements of the Borrmann fan intensities are shown in Fig. 5(*b*). With the analyser set to $\alpha = 45$ and $\alpha = 135°$, it was selective to the π and the σ components, respectively. A drastic reduction of the background level is observed compared with the measurements without the analyser and the *Pendellösung* oscillations are more clearly visible. This fact is caused mainly by the polarization-sensitive detection and also by the angle sensitivity of the Bragg reflecting analyser crystal. For visual reasons, both curves in Fig. 5(*b*) are normalized to unity. A comparison of the two curves in order to determine the value of the ratio of intensity for both perpendicularly polarized wavefields from these curves will fail because the divergence of the radiation was not constant for different azimuthal values. Thus, the maximum intensities of the analyser crystal that are measured in Fig. 5(*b*) must be corrected by a factor that takes into account the different divergences for different azimuthal angles around the beam. This problem will be overcome by measurement of the integrated intensities at each azimuthal position.

4.2. *Determination of the polarization state*

Firstly, the polarization state of incoming linearly polarized synchrotron radiation was measured for checking the analyser arrangement. The beam passed both slits (slit 2 in maximum intensity position) and the sample crystal, which was out of the Laue condition by 1°. The measurement of the degree of linear polarization of the undiffracted beam gives *ca* 92.5%. This was determined using the relation $P = [I(\alpha = 0°) - I(\alpha = 90°)]/[I(\alpha = 0°) + I(\alpha = 90°)]$. The intensity $I(\alpha = 0)$ corresponds to the scattered intensity of the radiation with the electric field vector in the orbit plane. The incomplete linear polarization of the beam is caused by the mixing of the circularly polarized components with opposite helicity coming from regions above and below the orbit plane of the storage ring (Shen & Finkelstein, 1993).

The presented method for analysis of the polarization state is only sensitive to the linearly polarized parts of the beam. One cannot distinguish between unpolarized and circularly polarized radiation and it is not possible to determine the helicity of the radiation. In order to determine the full polarization state of the beam (amplitude and phase), *e.g.* in the form of the three Stokes's parameters, one must add a quarter-wave plate to this analyser arrangement (Giles, Malgrange *et al.*, 1995; Giles, Vettier *et al.*, 1995). Another way is to additionally use a multiple-beam polarimeter as reported by Shen (1993). Nevertheless, the use of the presented arrangement is justified by assuming that no depolarization effects occur in the perfect sample crystal.

The quantitative determination of the polarization state from the measured data was made by fitting a model function to the measured curves. It is supposed in the following that the incident radiation is linearly polarized. The time-averaged amplitude distribution of an arbitrarily but completely polarized wave can be described by the superposition of two mutually perpendicularly polarized waves, which have amplitudes $D_{\sigma(\pi)}$ and phase difference Φ. The polarization ellipse in a Cartesian $(\varepsilon_1; \varepsilon_2)$ coordinate system is given by the parameter representation:

$$\varepsilon_1 = R \sin \tau, \quad \varepsilon_2 = \sin(\tau - \Phi). \tag{4}$$

Here, $R = D_\sigma/D_\pi = (I_\sigma/I_\pi)^{1/2}$ is the ratio of the amplitudes of these waves. A polarization ellipse can be fitted to the measured data for a completely polarized beam. One has to take into account that two wavefields (1) and (2) are exiting in the crystal simultaneously as shown before. They have opposite helicities and different amplitudes. For this reason, the fitting function must be completed by a second wave taking into account the anomalously strongly absorbed wavefield with the amplitude sR and a phase difference between the two perpendicularly polarized waves of $-\Phi$. Here, the quantity $s = (I_2/I_1)^{1/2}$ is the ratio of amplitudes of the wavefields (2) and (1) for the same polarization state (see Fig. 3). The corrected parameter representation of the polarization ellipse follows:

$$\varepsilon_1 = R(1 + s) \sin \tau, \quad \varepsilon_2 = \sin(\tau - \Phi) + s \sin(\tau + \Phi). \tag{5}$$

Here, τ is a parameter in the range $0 \leq \tau \leq 2\pi$. In the case of thick absorbing crystals, only the weakly absorbed wavefield contributes to the transmitted intensity. In this case, the quantity s is zero. For $s = 1$, both wavefields have equal amplitudes and linear polarization occurs for any value of R and Φ but the polarization plane is rotated in relation to both parameters. For the measured data points the value of s was calculated according to Authier (1961) (see Fig. 3). In order to compare the experimental results of $I(\alpha)$ with the calculations using (5), the calculated polarization ellipse must be convoluted by the $\cos^2$ function taking into account the acceptance of the analyser. The fitting curves and the measured data are normalized to unity.

The polar plot in Fig. 6(*a*) shows the amplitude distribution of a polarization ellipse of a linearly polarized wave where the polarization plane is in the orbit plane as a function of the angle α. Additionally, it

shows the intensity distribution $I(\alpha)$ after convolution with Malus's $\cos^2$ law, which is measurable by a polarization analyser with a scattering angle of 90°, as used in the experiment. In the case of linear polarization in the orbit plane, the ratio of amplitudes R is unity and the phase difference Φ is zero.

The sample was adjusted into the Laue position for the determination of the local resolved polarization state inside the Borrmann fan. The polarization state was measured for several positions in the Borrmann fan as described in the experimental section. The normalized integrated intensities $r = I(\alpha_{max})/I(\alpha)$, which were measured at $x + x_{BF} = 66\,\mu m$, are plotted against the azimuthal angle α in Fig. 6(*b*). A significant change of the polarization state compared with that of the incident radiation is observed. The fitting parameters in (5) were determined as $\Phi = 260°$ and $R = 1.3$, assuming a value of $s = 0.3$ (calculation gives $\Phi_c = 257°$ and $R_c = 1.6$). The polarization ellipse that is drawn in the same figure (dashed line) symbolizes the time-averaged amplitude distribution of the electric field vector of the wave. The eccentricity of the ellipse is mainly caused by the ratio of the amplitudes of both linearly polarized components, which differs from unity strongly, and also by the large phase shifting, which is almost $3/2\pi$. In the polar plots of Fig. 7, further results for polarization analysis at positions $x + x_{BF} = 35$, 87 and 108 μm are shown.

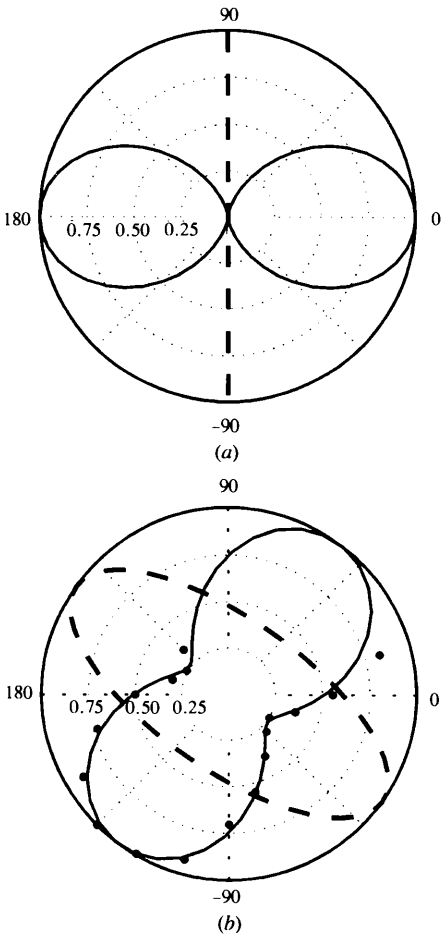

Fig. 6. (*a*) Polar representation of the polarization ellipse for an almost polarized wave (dotted line) with $\Phi = 0°$ and $R = 1$. The solid line is the normalized intensity distribution $r(\alpha) = I(\alpha_{max})/I(\alpha)$ scattered perpendicular to the direction of the beam. (*b*) Polar representation of the normalized intensities $r(\alpha) = I(\alpha_{max})/I(\alpha)$ of the measured data points (•) for slit 2 at $(x + x_{BF}) = 66\,\mu m$. The solid line gives the calculated azimuthal intensity distribution for a fit of equation (5): $R = 1.3$ {1.6}; $\Phi = 260°$ {257°} with $s = 0.3$. The dotted line is the polarization ellipse resulting from the fitting parameters. The values in curly brackets are the values from the dynamical theory.

The main reason for the partial disagreement of calculations and experiment is the uncertainty caused by the strong variation of the intensity with the position of the second slit. The intensity ratio changes very rapidly outside the centre of the Borrmann fan (see Fig. 2). Even a small deviation from a position x of some μm or a small deviation of the measured thickness of the crystal will change the parameter R. The change of phase shifting with the position in the Borrmann fan has an additional but weaker influence. The inexact linearly polarized incident radiation also cannot cause the partially large deviations from the expected values.

From the calculations, it is evident that, in the centre of the Borrmann fan, R and Φ have only small changes with position. There the polarization state can be measured with smaller errors.

5. Summary

The present experiment was performed in order to verify the local variation of the polarization state in the forward-diffracted beam in Laue-case X-ray diffraction. The experimental and theoretical results show that the polarization state of linearly polarized X-rays changes in a complicated way. The drastic variation of both the phase retardation and the amplitude ratio of the wavefields makes the polarization state very sensitive to changes in the experimental parameters, such as positions of the slit, thickness of the crystal or inclination of the diffraction plane against the polarization plane of the incident linearly polarized wave. The transmitted intensity decreases drastically by the use of two narrow slits. For this reason, it will not be useful to apply the presented experimental arrangement for the generation of arbitrarily polarized X-rays with sufficient intensity. More effective methods, such as the transmission-phase retarder in Bragg or in Laue geometry, can be used (Hirano *et al.*, 1991; Giles *et al.*, 1994).

The experiment was carried out with an incident divergent radiation exiting the whole dispersion surface. Owing to the narrow second slit, only a small region of the dispersion surface is selected at

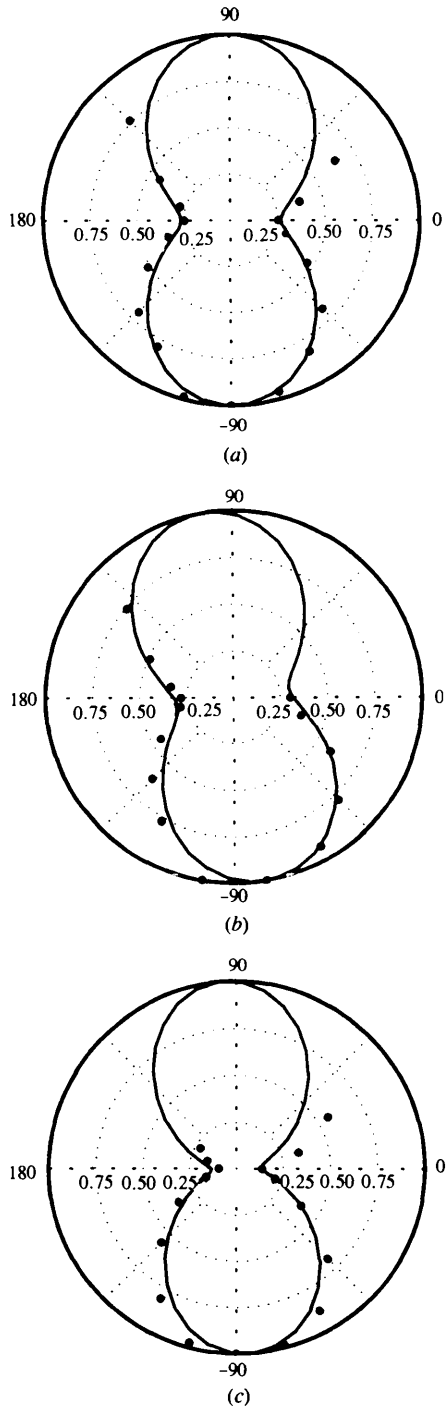

Fig. 7. Polar representation of the normalized intensities $r(\alpha) = I(\alpha_{max})/I(\alpha)$ of the measured data points (•) for slit 2 at different positions in the Borrmann fan. The solid lines give the calculated azimuthal intensity distribution for the best fit using equation (5). Fit results: (*a*) $(x + x_{BF}) = 35\,\mu m$: $R = 0.6$ {0.9}; $\Phi = 242°$ {215°} with $s = 0.34$; (*b*) $(x + x_{BF}) = 87\,\mu m$: $R = 0.55$ {1.6}; $\Phi = 245°$ {245°} with $s = 0.32$; (*c*) $(x + x_{BF}) = 108\,\mu m$: $R = 0.65$ {1.0}; $\Phi = 230°$ {210°} with $s = 0.37$. The values in curly brackets are the values from the dynamical theory.

the exit surface. Therefore, this experiment is analogous to an experiment with an incident plane wave where the polarization state depends on the deviation from the exact Bragg angle. In most conventional experiments, the angular-resolved modification of the polarization state cannot be seen because an integration over all the states (excitation of the whole dispersion surface) takes place. The results of the experiment and the presented method may be interesting for experiments with highly collimated synchrotron radiation of third-generation sources.

This work was supported by the BMFT under project no. 5NHAAB0. We thank K. Eichhorn, H. G. Krane and J. Weigelt for their help at HASYLAB, Hamburg, and V. Alex and K. Nippe from IKZ Berlin for manufacturing the Si plates.

References

Authier, A. (1961). *Bull. Soc. Fr. Minéral. Cristallogr.* **84**, 51–89.

Authier, A. (1970). *Advances in Structure Research by Diffraction Methods*, Vol. 3, edited by R. Brill & R. Mason, pp. 1–51. Oxford: Pergamon Press; Braunschweig: Vieweg.

Belyakov, V. A. & Dmitrienko, V. E. (1989). *Sov. Phys. Usp.* **32**, 697–719.

Brümmer, O., Eisenschmidt, C. & Höche, H. R. (1982). *Z. Naturforsch. Teil A*, **37**, 524–527.

Cole, H., Chambers, F. W. & Wood, C. G. (1961). *J. Appl. Phys.* **32**, 1942–1945.

Giles, C., Malgrange, C., Goulon, J., de Bergevin, F., Vettier, C., Dartyge, E., Fontaine, A., Giorgetti, C. & Pizzini, S. (1994). *J. Appl. Cryst.* **27**, 232–240.

Giles, C., Malgrange, C., Goulon, J., de Bergevin, F., Vettier, C., Fontaine, A., Dartyge, E., Pizzini, S., Baudelet, F. & Freund, A. (1995). *Rev. Sci. Instrum.* **66**, 1549–1553.

Giles, C., Vettier, C., de Bergevin, F., Malgrange, C., Grübel, G. & Grossi, F. (1995). *Rev. Sci. Instrum.* **66**, 1518–1521.

Hart, M. & Lang, A. R. (1965). *Acta Cryst.* **19**, 73–77.

Hattori, H., Kuriyama, H. & Kato, N. (1965). *J. Phys. Soc. Jpn*, **20**, 1047.

Hirano, K., Ishikawa, T. & Kikuta, S. (1993). *Nucl. Instrum. Methods Phys. Res.* A**336**, 343–353.

Hirano, K., Ishikawa, T., Nakamura, I., Mizutani, M. & Kikuta, S. (1994). *Jpn. J. Appl. Phys.* **33**, L689–692.

Hirano, K., Izumi, K., Ishikawa, T., Anaka, S. & Kikuta, S. (1991). *Jpn. J. Appl. Phys.* **30**, L407–410.

Kato, N. (1961). *Acta Cryst.* **14**, 526–532, 627–636.

Kato, N. & Lang, A. R. (1959). *Acta Cryst.* **12**, 787–794.

Shen, Q. (1993). *Acta Cryst.* A**49**, 605–613.

Shen, Q. & Finkelstein, K. D. (1993). *Rev. Sci. Instrum.* **64**, 3451–3455.

Skalicky, P. & Malgrange, C. (1972). *Acta Cryst.* A**28**, 501–507.

Takagi, S. (1969). *J. Phys. Soc. Jpn*, **26**, 1239–1253.